Supplementary information

Elucidating the effects of carbon source on fluorination kinetics and the CF_x structure to tailor the energy density of Li/CF_x

Shixue Zhang,[a] Yu Li,[a] Hang Xu,[a] Cong Peng,[a] Lingchen Kong,[b] Zhihao Gui,[a] and Wei Feng*[ab]

[a] *Institute of Advanced Technology and Equipment, Beijing University of Chemical Technology, 100029, Beijing, China.*
[b] *School of Materials Science and Engineering and Tianjin Key Laboratory of Composite and Functional Materials, Tianjin University, 300072, Tianjin, China.*
* *E-mail: weifeng@tju.edu.cn*

1. Experimental section

1.1 Material preparation

Fluffy carbon was prepared via pre-oxidation and carbonisation. Clean rice (GB/T 1354-2018, starch content 76.9 %, protein content 8.1 %, Old Taste Food Factory) was dipped in water for 4 h, dried at 25 °C, sealed in a high-pressure-resistant container, baked in a fire for 10–15 min and quickly opened to obtain puffed rice. During this puffing process, the internally sealed air expanded the cavity, and the in-cell water vapor stretched the interlayer, forming new pores and reducing the thickness of the wall. The puffed rice was spread in a large Petri dish and placed in a blast oven at 230 °C for 8 h. The temperature was set according to the TG analysis of puffed rice (**Fig. S1**).[1] This pre-oxidisation process was required to ensure that the hydroxyl groups on the glucose unit were oxidised to carbonyl, aldehyde and carboxyl groups, and a highly cross-linked network structure could be obtained via polymerisation and cross-linking between molecular chains.[2, 3] The fluffy structure was preserved during carbonisation in a tube furnace at 800 °C under an Ar atmosphere for 2 h (**Fig. S2**). The resulting sample (fluffy-A0) was then activated using H_2O etching at 800 °C for 60, 90 and 120 min (4.2 mL min^{-1}) to form a series of HPCs. The specific morphology and pore size distribution were related to the activation time, and the obtained samples were labelled fluffy-A60, fluffy-A90 and fluffy-A120.

Direct fluorination was used to fluorinate the fluffy-A0 and HPCs. The thin wall that was regulated by the puffing process was conducive to form more through-pores during activation, thereby further enhancing fluorine diffusion (**Fig. S3**). To reveal the synergistic effect of the fluorination temperature and carbon source on the structure of formed CF_x and the impact on the performance, an orthogonal experiment was designed. The obtained fluffy-A0 and HPCs were reacted with N_2/F_2 (8:2) for 5 h in a custom-made Monel reactor at 120, 160, 200 and 240 °C. Notably, grinding the carbon source before fluorination decreased the fluorination time. The formed CF_x was labelled Ax-Fy, where x and y represent the activation time and fluorination temperature, respectively.

1.2 Electrochemical characterisation

Coin cell: The electrode was prepared by mixing the synthesised fluorinated samples (80 wt%), Ketjenblack EC-300J (10 wt%) and polyvinylidene fluoride binder (10 wt%) in N-methyl-2-pyrrolidone (NMP) to form a homogeneous slurry, which was then coated on Al foil and vacuum dried at 120 °C for 12 h. The dry foil was subsequently transferred to an Ar-filled glove box and cut into shapes suitable for coin cells. The average electrode load was approximately 1 mg cm^{-2}. Standard Li/CF_x coin cells were prepared with the above-mentioned working electrode, a 14 μm three-layer PP-PE-PP membrane, a 0.4 mm Li foil counter electrode and 1 M LiFSI in PC/DME (1:1 by volume). The galvanostatic discharge of the coin cells was performed on a LAND CT-2001A (Wuhan, China) test system with a voltage window between the open-circuit voltage

and 1.5 V, and the discharge rate was calculated using a theoretical capacity of 865 mAh g^{-1}. In order to test the potential of the active material (formed CF_x), the coin cell was used. The calculation of energy density and specific capacity was based on the mass of the active material. Electrochemical impedance spectroscopy of the cells was measured using a CHI660E Chenhua electrochemical workstation (Shanghai, China) in the frequency range of 0.01–10^5 Hz at 3.0 V.

Pouch cell: The cathode slurry was prepared with A90-F160 (88 wt%), Super P (6 wt%), polymerised styrene butadiene rubber (SBR, 3 wt%), carboxymethyl cellulose (CMC, 3 wt%) and deionised water. The cathode electrode was prepared by double-coating the slurry onto Al foil. Subsequently, the electrodes were vacuum dried at 120 °C for 12 h, cut into 4 × 5.5 cm^2 rectangles and weighed to calculate the mass loading, which was approximately 15–20 mg cm^{-2}. The pouch cell was assembled by stacking the cathode and lithium anode with a separator, encapsulating them in an Al–plastic film and injecting the electrolyte (1 M LiFSI in PC/DME (1:1 by volume)).

1.3 Characterisations

The morphology of the obtained samples was observed using SEM (ZEISS Gemini 300, Oberkochen, Germany), and TEM (JEOL JEM-F200, Tokyo, Japan) was used to obtain TEM images and the corresponding diffraction patterns. The structure of the synthesised material was characterised using XRD (Rigaku-2038, Tokyo, Japan) equipped with Cu kα radiation. The specific surface areas and hierarchical pore structures of the samples were calculated using the Brunauer–Emmett–Teller (Micromeritics APSP2460) method. FTIR analysis was used to identify the functional groups of the prepared materials using a Thermo Scientific Nicolet iS20 spectrometer (Massachusetts, USA) in the range of 1000–2000 cm^{-1}. The surface chemical information of the obtained samples was confirmed using XPS (Thermo Scientific ESCALAB Xi+, Massachusetts, USA) with an Al kα monochromatic source. The depth profile was obtained to characterise the valence state of the subsurface regions. In particular, the XPS signals were continuously collected after etching the materials layer-by-layer using low-energy Ar^+ with 5 nm intervals of sputtering. TG and differential TG (DTG) curves were analysed using a NETZSCH STA 2500 (Selb, Germany).

1.4 Theoretical calculations

DFT calculations were performed using the Vienna Ab initio Simulation Package with generalised gradient approximation using the Perdew–Burke–Ernzerhof functional.[4-6] Projector-augmented wave pseudopotentials were selected, valence electrons were considered and a plane–wave basis set with a kinetic energy cutoff of 450 eV was used.[7, 8] The lattice parameter of graphene and the size of the supercell were 8 × 8 × 1 and 19.68 Å × 19.68 Å × 20 Å, respectively, as shown in the charge density differences of F-PG and F-VG (**Fig. S4**). Geometry optimisations were performed with a force convergence <0.05 eV $Å^{-1}$. A climbing image-nudged elastic band method was used to

locate transition states using the same convergence standard.[9, 10] The spin-polarisation effect was also considered. The DFT-D3 empirical correction method was used to describe the van der Waals interactions. All atoms were relaxed during the calculations.

1.5 Calculation of the diffusion coefficient

The diffusion coefficient (D_{Li^+}) of Li^+ was calculated using the GITT profile.[11] The coin cells with the A0-F160 and FHPCs cathodes were discharged at 0.1 C for 10 min, followed by resting to ensure the voltage reached a steady state (40 min). A significant linear relationship (R^2 >0.99) between the transient voltage and $\tau^{1/2}$ is shown within the range of 10–50 s (**Fig. S5**). Therefore, the diffusion coefficient of Li^+ was calculated with the simplified equation using Fick's second law:

$$D_{Li^+} = \frac{4}{\pi}\left(I_0 \frac{V_m}{SFZ_i}\right)^2 \left(\frac{dE/dx}{dE/d\tau^{\frac{1}{2}}}\right)^2 \quad \left(\tau \ll L^2/D_{Li^+}\right) \qquad \textbf{Equation S1}$$

where I_0 is the current, V_m is the molar volume of the active material, F is the Faraday constant, S is the contact area between the electrolyte and electrode, Z_i is the charge transfer number during the discharge process of the Li/CF_x battery and L is the thickness of the electrode.

2. Supporting figures

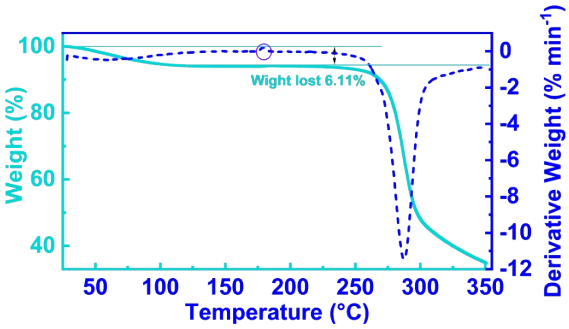

Fig. S1. TG-DTG curve of puffed rice from RT to 350 °C under an air atmosphere.

The slight weight loss starts at 25 °C, which is mostly due to the likely presence of residual adsorbed water. As the temperature rises to around 160 °C, a slight weight gain can be seen, which may be due to the acquisition of oxygen. This process only lasted for a short temperature window, and till about 230 °C, the total weight loss reached 6.11 %. Then evidently weight loss can be observed at 276°C, indicating a rapid decomposition process.[12] Based on the TGA results, 230 °C was chosen as the pre-oxidation temperature.

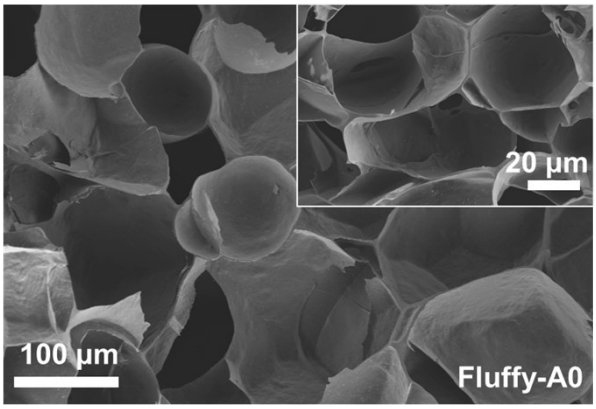

Fig. S2. The SEM of carbonized puffed-rice, which named as fluffy-A0 in the main text.

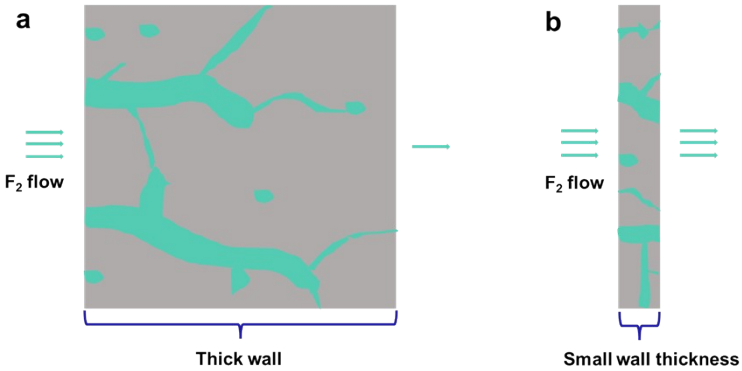

Fig. S3. The schematic diagram of the hierarchical pore structures after water steam activation of carbonized rice (a) and puffed rice (b), and the consequent influence on the diffusion of gaseous fluorinating agent (F_2).

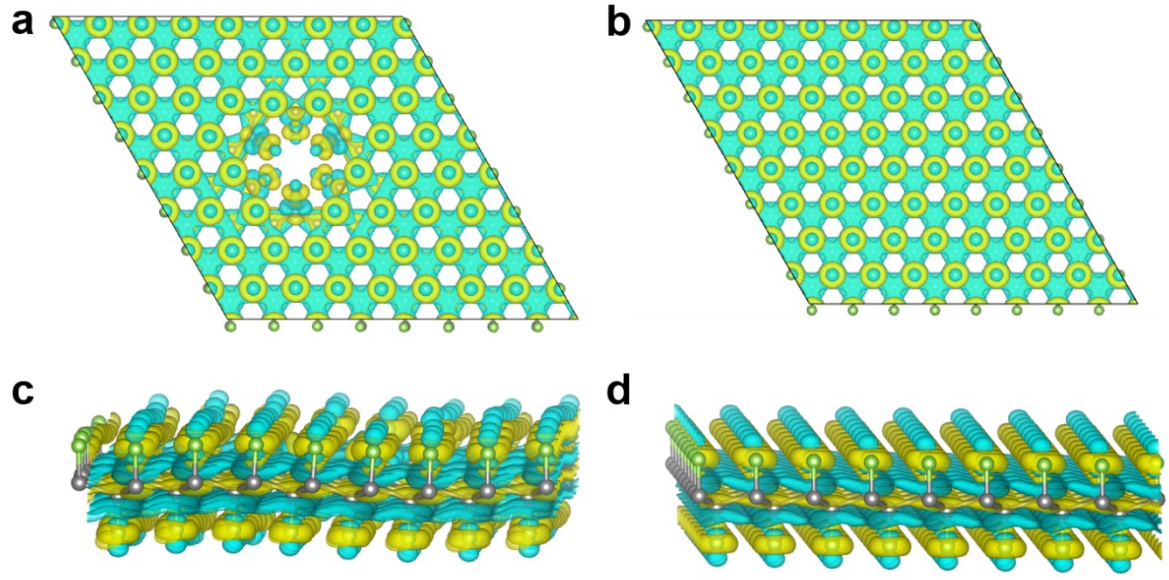

Fig. S4. Top and side view of charge density differences of F-VG (a, c) and F-PG (b, d). Yellow corresponds to charge accumulation and blue corresponds to charge depletion with an isovalue of 0.01 e/bohr^3.

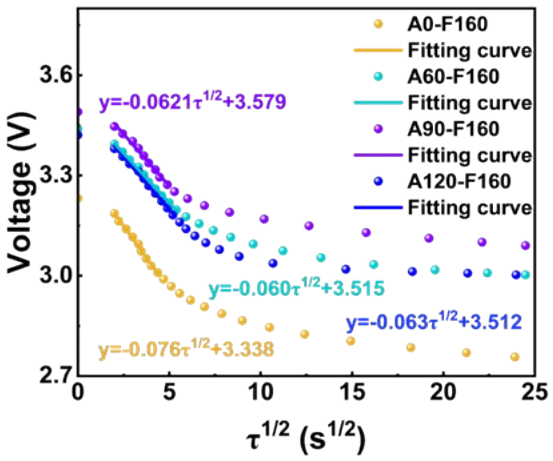

Fig. S5. The transient voltage changes along with $\tau^{1/2}$ during a single titration process. A significant linear relationship is shown within the range of 10-50 s.

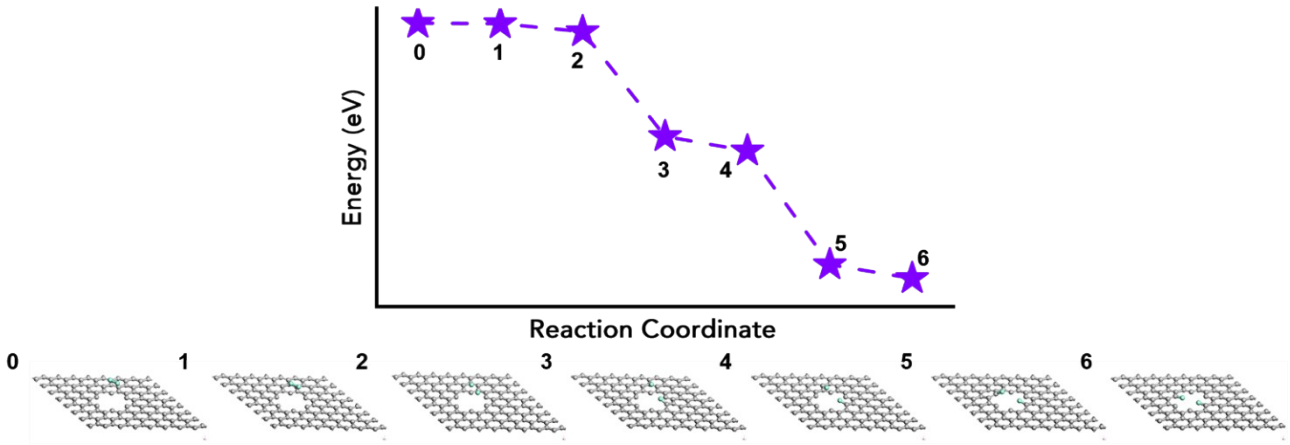

Fig. S6. Reaction mechanism and energy of reaction (ΔE_R) of graphene with vacancy (VG) that is fluorinated by F_2. The positions of F atoms in each step during the fluorination reaction are posted below, where gray spheres represent carbon atoms and light blue spheres represent fluorine atoms.

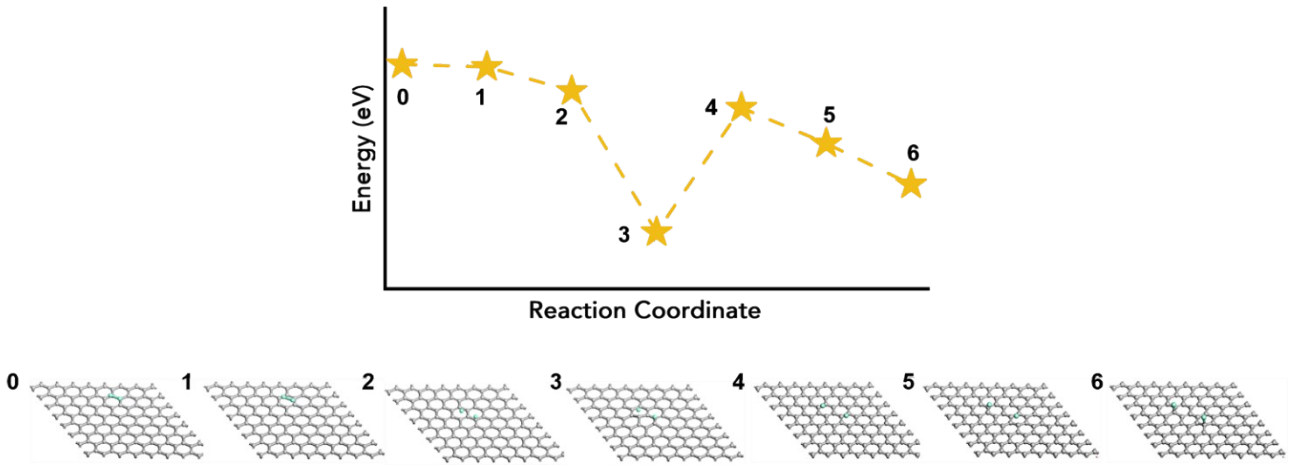

Fig. S7. Reaction mechanism and energy of reaction (ΔE_R) of perfect graphene (PG) that is fluorinated by F_2. The positions of F atoms in each step during the fluorination reaction are posted below, where gray spheres represent carbon atoms and light blue spheres represent fluorine atoms.

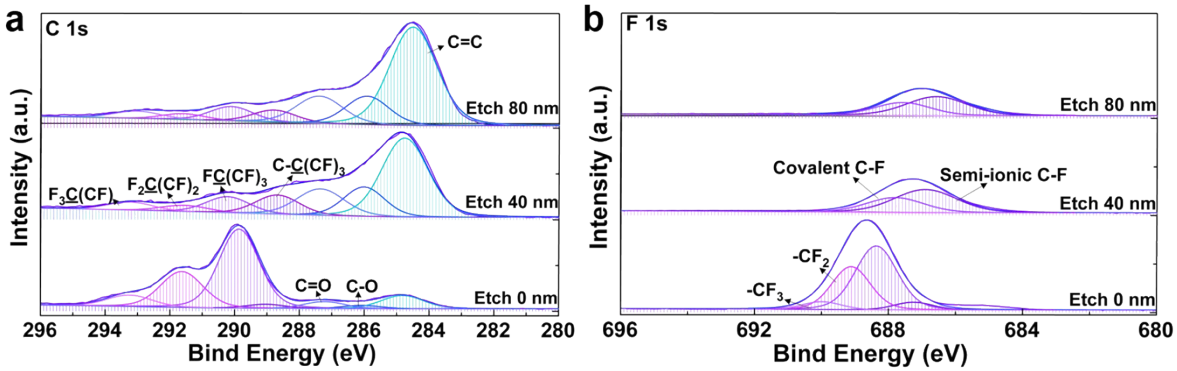

Fig. S8. XPS peak differentiation imitating analysis of C 1s (a) and F 1s (b) during different sputtering depths of A0-F160.

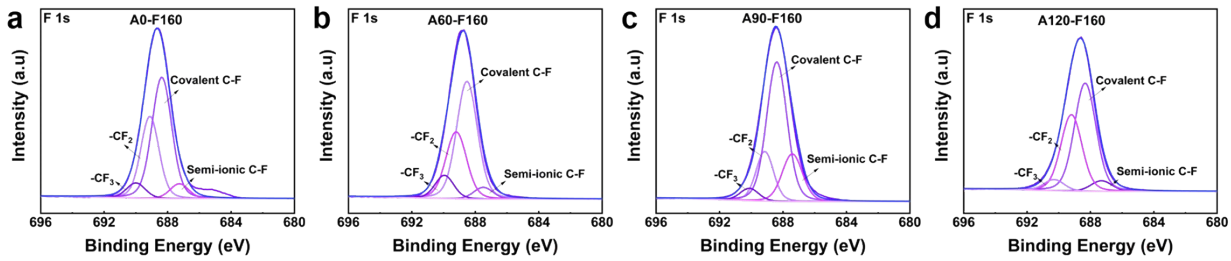

Fig. S9. XPS peak differentiation imitating analysis of F 1s of A0-F160 (a), A60-F160 (b), A90-F160 (c) and A120-F160 (d).

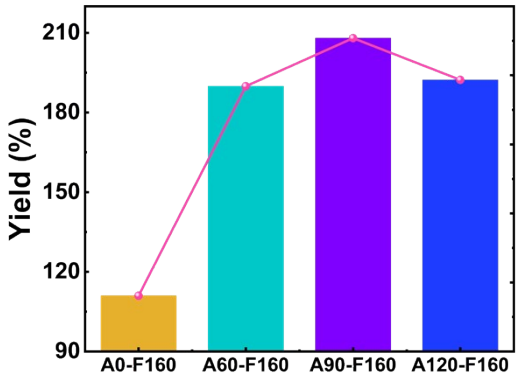

Fig. S10. The yield comparison of fluorinated samples with different carbon sources that fluorinated at the same condition.

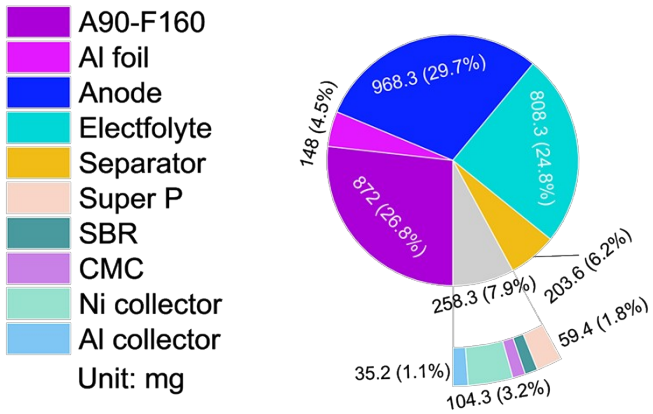

Fig. S11. The mass and mass proportion of the battery component in the pouch cell.

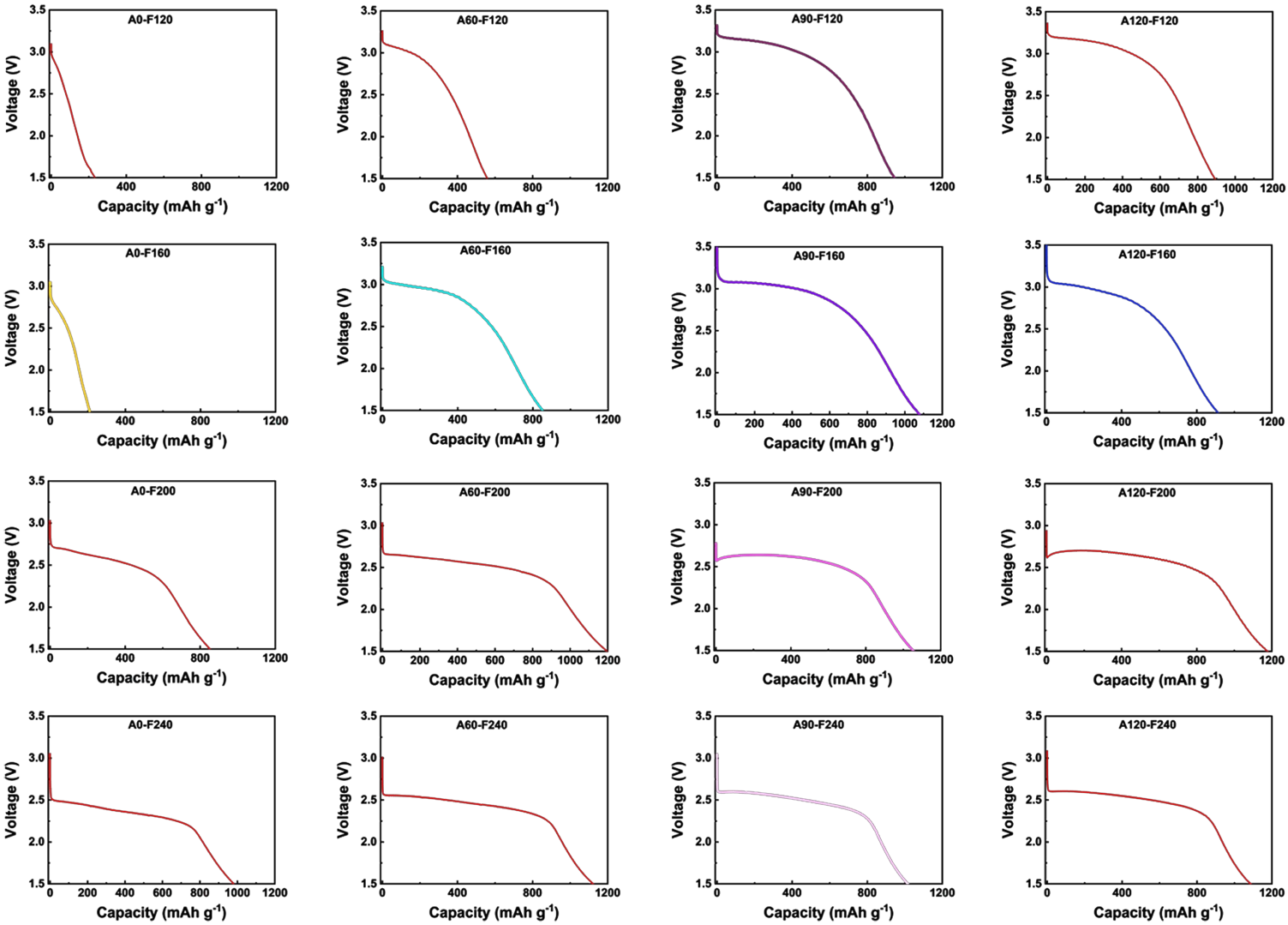

Fig. S12. The discharge profile of all samples that tested in this orthogonal experiment, all the Li/CF_x batteries were tested at room temperature (25°C) with a current density of 0.05 C.

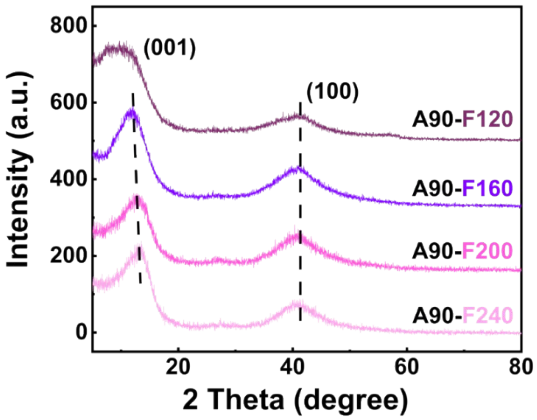

Fig. S13. The XRD curves of fluffy-A90 that fluorinated with temperatures of 120, 160, 200, 240 °C.

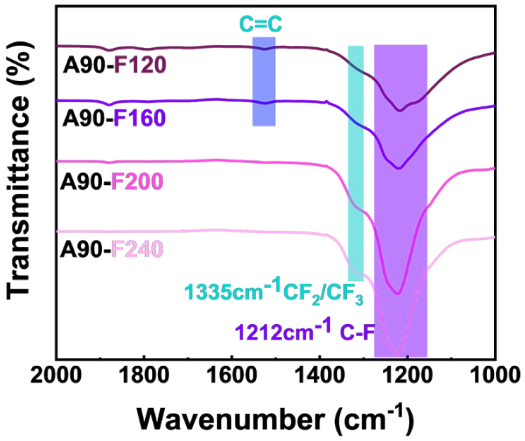

Fig. S14. Infrared absorption spectra of fluffy-A90 that fluorinated with various temperatures.

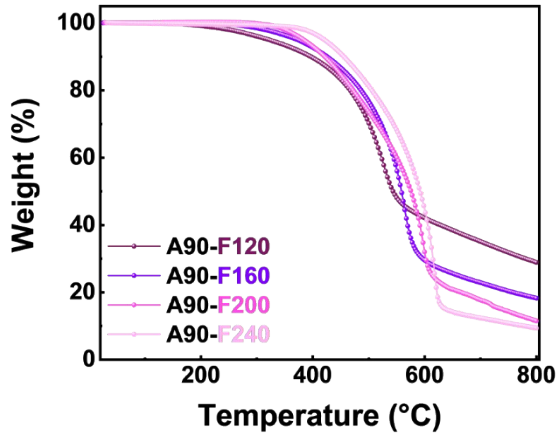

Fig. S15. The TG curves of fluffy-A90 that fluorinated with various temperatures.

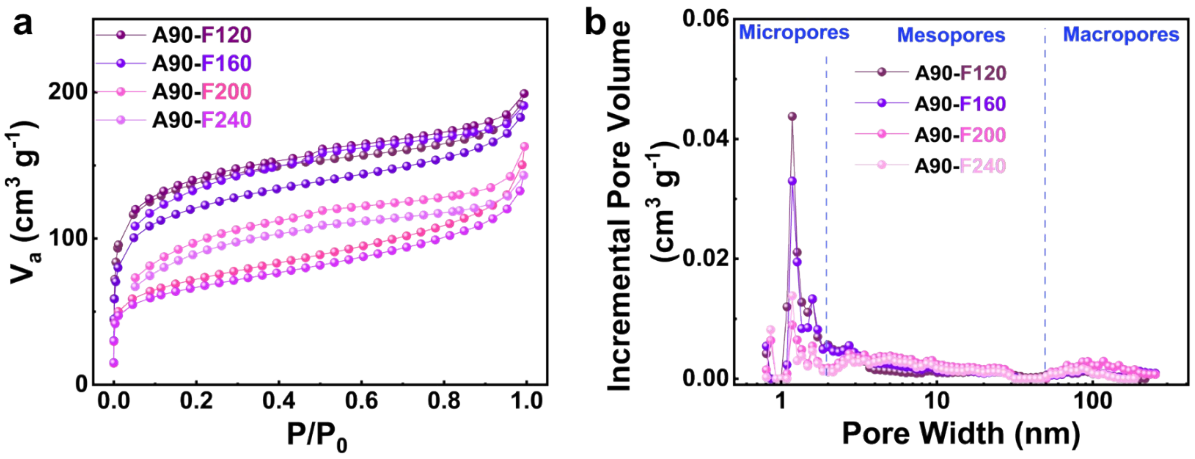

Fig. S16. N_2 adsorption/desorption isothermal curves of A90-F120, A90-F160, A90-F200 and A90-F240 (a), and their pore size distribution curves calculated by original density functional theory (b).

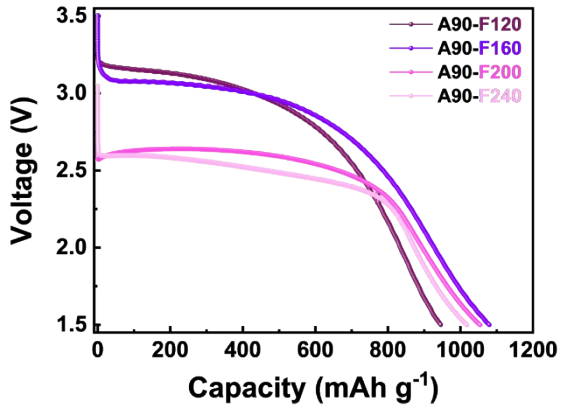

Fig. S17. Discharge charge profile of fluffy-A90 that fluorinated with various temperatures.

3. Supporting tables

Table S1. Detailed structural information of the fluffy carbon (fluffy-A0) and HPCs water-steam activation.

Carbon source	S_{BET} [$m^2\ g^{-1}$][a)]	V_{tot} [$cm^3\ g^{-1}$][b)]	D_{ave} [nm][c)]	S_{mic} [$m^2\ g^{-1}$][d)]	S_{BJH} [$m^2\ g^{-1}$][e)]
fluffy-A0	820.96	0.356	1.73	765.03	61.02
fluffy-A60	1399.03	0.689	1.97	1148.01	263.97
fluffy-A90	1542.36	0.785	2.035	1202.92	351.09
fluffy-A120	1555.45	0.856	2.20	1293.75	468.03

[a)] The Brunauer-Emmett-Teller (BET) surface area.

[b)] The total pore volume (P/P_0 = 0.950).

[c)] The average pore sizes by BET.

[d)] The specific surface area of micropores by the t-plot method.

[e)] The specific surface area of mesopores by BJH method (1.7-300nm).

Table S2. The interlayer space of carbon sources and formed CF_x (obtained from XRD results).

Carbon source	**2θ [°]**	**d (002) [Å]**	**Sample**	**2θ [°]**	**d (001) [Å]**
fluffy-A0	22.83	3.89	A0-F160	11.19	7.9
fluffy-A60	22.37	3.97	A60-F160	11.58	7.63
fluffy-A90	22.26	3.99	A90-F160	11.98	7.38
fluffy-A120	22.22	3.99	A120-F160	11.99	7.37

Table S3. Chemical composition analysis of the formed CF_x.

T [°C] (fluorination)	Carbon source	Sample	Atom C [%]	Atom F [%]	Atom O [%]	F/C Ratio (XPS)	F/C Ratio (TG)
160	fluffy-C	A0-F160	43.33	54.1	2.57	1.25	0.12
	fluffy-A60	A60-F160	41.94	55.05	3.01	1.31	1.00
	fluffy-A90	A90-F160	44.98	50.76	4.26	1.13	1.10
	fluffy-A120	A120-F160	42.14	55.67	2.19	1.32	1.35

$$R_{F/C} = \frac{|W_1 - W_2|/Ar(F)}{W_2/Ar(C)}$$

Equation S1

In the **Equation S1**, W_1 (W_2) is the residual weight at the end of the first (second) stage, Ar (C) and Ar (F) are the relative atomic masses of C and F, respectively.

Table S4. The proportion results of the XPS peak differentiation analysis of C 1s and F 1s.

Sample	C 1s assignment [eV]						
	C-C/C=C [%]	**Semi-ionic C-F [%]**	**C-F [%)**	**CF_2 [%]**	**CF_3 [%]**	**C-O [%]**	**C=O [%]**
A0-F160	284.8	289	289.9	291.6	293.2	286.1	287.2
	8.96	2.50	49.90	24.06	8.13	1.99	4.46
A60-F160	284.7	289	290	291.7	293.2	286.3	287.4
	2.27	4.56	58.06	21.17	7.09	0.82	6.04
A90-F160	284.5	289.1	289.9	291.6	293.3	286.2	287.4
	12.04	12.43	42.43	17.55	4.04	4.90	6.62
A120-F160	284.5	288.9	289.9	291.5	293.2	286.1	287.2
	4.92	6.32	51.12	24.95	6.06	1.49	5.15

Sample	F 1s assignment [eV]			
	Semi-ionci C-F [%]	**C-F [%]**	**-CF_2 [%]**	**-CF_3 [%]**
A0-F160	687.1	688.4	689.1	689.9
	5.77	54.21	33.70	6.33
A60-F160	687.5	688.5	689.2	689.9
	4.95	54.43	30.98	9.64
A90-F160	687.4	688.4	689.1	690.1
	19.72	57.98	17.70	4.60
A120-F160	687.3	688.3	689.2	690.2
	5.03	53.09	36.79	5.09

Table S5. Statistics on the yield of the formed CF_x.

Carbon source	Sample	Yield [%]
fluffy-A0	A0-F160	111
fluffy-A60	A60-F160	197.9
fluffy-A90	A90-F160	208
fluffy-A120	A120-F160	192.3

Table S6. The electrochemical performance of the formed CF_x in the orthogonal experiment.

Carbon Source	Sample	T [°C] (fluorination)	Energy Density [Wh kg^{-1}]	Voltage [V]	Capacity [mAh g^{-1}]
fluffy-A0	A0-F120	120	517.09	2.19	234.77
	A0-F160	160	490.22	2.41	212.61
	A0-F200	200	2013.1	2.5	853.42
	A0-F240	240	2202.47	2.33	982.29
fluffy-A60	A60-F120	120	1454.6	2.79	560.06
	A60-F160	160	2215.84	2.82	853.21
	A60-F200	200	2847.16	2.56	1198.48
	A60-F240	240	2616.63	2.44	1123.99
fluffy-A90	A90-F120	120	2602.75	2.96	945.9
	A90-F160	160	2902.45	2.92	1079.83
	A90-F200	200	2541.43	2.58	1054.11
	A90-F240	240	2411.13	2.48	1017.87
fluffy-A120	A120-F120	120	2482.07	3	894.52
	A120-F160	160	2392.12	2.83	914.24
	A120-F200	200	2876.71	2.6	1179.87
	A120-F240	240	2588.52	2.5	1086.47

Table S7. The electrochemical performance of previous studies.

NO.	Ref.	Carbon source	Abbreviations	Capacity [mAh g^{-1}]	Current density	$E_{1/2}$ [V]	Energy density [Wh kg^{-1}]
1	13	Hard carbon (HC)	HC	922.6	0.01C	2.7	2466
2	14	honeycomb N-doped graphene	HNG	923.79	0.01C	3.04	2595.47
3	15	helical carbon nanotubes	HCNT	794.4	0.01C	2.9	2133.13
4	16	microporous carbon spheres	MCS	955	0.01C	2.74	2428
5	17	Multi-layered graphene	Mlgraphene	852*	10mA/g	2.75*	2239.8
6	18	hard carbon (HC)	HC-2	900	10mA/g	2.3*	2059
7	19	nanographite	nanographite	837.4	10mA/g	2.54	2004.5
8	20	nut shell	nut shell	949	10mA/g	2.98	2585
9	21	carbon nanotubes	CNT	939.2	10mA/g	3	2738.45
10	22	graphite oxyfluorides	OFG	1140*	10mA/g	2.5	2825
11	23	fluorinated activated needle-coke	FANC	789.5	50mA/g	2.82	2109.8
12	24	nanohorns	nanohorns	863.4	0.05C	2.71	2231.2
13	This work	fluffy carbon	FC	1079.83	0.05C	2.92	2902.45
14	25	oriented carbon nanotube	OCNT	794.85	0.1C	2.25*	1754.79
15	26	graphene	graphene	800	0.1C	2.5	2000#
16	27	Ketjen Black (KB)	KB	750*	0.2C	2.96	2220#
17	28	graphene	graphene	869.6	0.1A/g	2.6*	2260.96#
18	29	multi-walled carbon nanotubes	MCNT	819.3	0.1A/g	2.6*	2050

Superscript * stands for data that is read from the corresponding performance figure.

Superscript # stands for data that was calculated by reading data based on a rectangular model, which leads to a possible overestimation.

References

1. X. Yang, S. Zhao, Z. Zhang, Y. Chi, C. Yang, C. Wang, Y. Zhen, D. Wang, F. Fu and R. Chi, *J Colloid Interface Sci*, 2022, **614**, 298-309.
2. J. H. Lin, H. Singh, J. Y. Ciao, W. T. Kao, W. H. Huang and Y. H. Chang, *Carbohydr Polym*, 2013, **92**, 1858-1864.
3. G. Zhang, L. Zhang, Q. Ren, L. Yan, F. Zhang, W. Lv and Z. Shi, *ACS Appl Mater Interfaces*, 2021, **13**, 31650-31659.
4. G. Kresse and J. Furthmüller, *Physical Review B*, 1996, **54**, 11169-11186.
5. G. Kresse and J. Furthmüller, *Comput. Mater. Sci*, 1996, **6**, 15-50.
6. J. P. Perdew, K. Burke and M. Ernzerhof, *Phys. Rev. Lett.*, 1996, **77**, 3865-3868.
7. P. E. Blöchl, *Physical Review B*, 1994, **50**, 17953-17979.
8. G. Kresse and D. Joubert, *Physical Review B*, 1999, **59**, 1758-1775.
9. H. Jónsson, G. Mills and K. W. Jacobsen, *Nudged elastic band method for finding minimum energy paths of transitions*, World Scientific, 1998.
10. V. Ásgeirsson and H. Jónsson, *Exploring Potential Energy Surfaces with Saddle Point Searches*, Springer International Publishing, Cham, 2020.
11. J. S. Horner, G. Whang, D. S. Ashby, I. V. Kolesnichenko, T. N. Lambert, B. S. Dunn, A. A. Talin and S. A. Roberts, *ACS Appl. Energy Mater.*, 2021, **4**, 11460-11469.
12. Y.-F. Du, G.-H. Sun, Y. Li, J.-Y. Cheng, J.-P. Chen, G. Song, Q.-Q. Kong, L.-J. Xie and C.-M. Chen, *Carbon*, 2021, **178**, 243-255.
13. R. Zhou, Y. Li, Y. Feng, C. Peng and W. Feng, *Compos. Commun.*, 2020, **21**, 100396.
14. L. Kong, Y. Li, C. Peng, L. Sun, K. Wang, Y. Liu and W. Feng, *Nano Energy*, 2022, **104**, 107905.
15. G. Chen, F. Cao, Z. Li, J. Fu, B. Wu, Y. Liu and X. Jian, *Nanotechnol. Rev.*, 2023, **12**, 20230108.
16. Y. Hu, L. Kong, W. Li, L. Sun, C. Peng, M. Qin, Z. Zhao, Y. Li and W. Feng, *Compos. Commun.*, 2023, **40**, 101607.
17. Y.-Y. Li, C. Liu, L. Chen, X.-Z. Wu, P.-F. Zhou, X.-Y. Shen and J. Zhou, *Rare Met.*, 2022, **42**, 940-953.
18. L. Chen, Y. Li, C. Liu, F. Guo, X. Wu, P. Zhou, Z. Fang and J. Zhou, *RSC Adv.*, 2023, **13**, 14797-14807.
19. L. Wang, Y. Li, S. Wang, P. Zhou, Z. Zhao, X. Li, J. Zhou and S. Zhuo, *ChemElectroChem*, 2019, **6**, 2201-2207.
20. C. Peng, Y. Li, F. Yao, H. Fu, R. Zhou, Y. Feng and W. Feng, *Carbon*, 2019, **153**, 783-791.
21. C. Peng, L. Kong, Y. Li, H. Fu, L. Sun, Y. Feng and W. Feng, *Sci. China Mater.*, 2021, **64**, 1367-1377.
22. M. Mar, M. Dubois, K. Guerin, N. Batisse, B. Simon and P. Bernard, *J. Fluorine Chem.*, 2019, **227**, 109369.
23. C. Liu, X. Wu, L. Chen, Y. Li, X. Wang, S. Chen, Z. Fang, J. Zhou and S. Zhuo, *J. Energy Storage*, 2024, **91**, 112024.
24. C. Peng, S. Zhang, L. Kong, H. Xu, Y. Li and W. Feng, *Small Methods*, 2023, **8**, e2301090.
25. J. Hou, X. Yang, X. Fu, D. Zou, J. Ma, Y. Peng, Y. Liu and X. Jian, *J. Alloys Compd.*, 2022, **923**, 166452.
26. Z. Luo, X. Wang, D. Chen, Q. Chang, S. Xie, Z. Ma, W. Lei, J. Pan, Y. Pan, J. Huang and J. Huang, *ACS Appl Mater Interfaces*, 2021, **13**, 18809-18820.
27. C. Wang, J. K. Teng, X. T. Chen, J. H. Wei, B. Shi, Z. F. Yuan, X. L. Li, S. S. Kang and K. K. Tang, *Energy Technol.*, 2023, **11**, 2300635.
28. H. P. Zhou, G. T. Chen, L. S. Yao, S. Zhang, T. T. Feng, Z. Q. Xu, Z. X. Fang and M. Q. Wu, *J. Alloys Compd.*, 2023, **941**, 168998.

29. L. S. Yao, H. P. Zhou, G. T. Chen, S. Zhang, T. T. Feng, Z. Q. Xu, Z. X. Fang, H. M. Zhang, L. Zhang and M. Q. Wu, *Diamond Relat. Mater.*, 2023, **131**, 109545.